A satellite perspective on cloud water to rain water conversion rates and relationships with environmental conditions

Armin Sorooshian,[1,2] Zhen Wang,[1] Graham Feingold,[3] and Tristan S. L'Ecuyer[4]

Received 19 February 2013; revised 23 May 2013; accepted 24 May 2013; published 26 June 2013.

[1] A two-year satellite remote sensing data set from the NASA A-Train is used to examine conversion rates of cloud water to rain water for warm maritime clouds with different ranges of mean cloud-layer radar reflectivity and rain rate. Recent work has demonstrated the utility of a novel procedure that relies on the differing sensitivities of passive MODIS measurements and active CloudSat radar measurements to estimate warm cloud conversion rates and associated time scales. That work is extended here to examine regional differences in conversion rates, including sensitivity to environmental parameters such as atmospheric stability and the presence of different aerosol types defined based on values of aerosol optical depth, fine mode fraction, and Ångstrom Exponent. Among eight subregions examined, the tropical Pacific Ocean is characterized by the highest average conversion rate while subtropical stratocumulus cloud regions (far northeastern Pacific Ocean, far southeastern Pacific Ocean, Western Africa coastal region) exhibit the lowest rates. Conversion rates are generally higher at reduced values of lower tropospheric static stability (LTSS). When examining data in two selected ranges for LTSS, higher conversion rates are coincident with higher LWP and factors covarying or rooted in the presence of aerosol types exhibiting lower aerosol index values.

Citation: Sorooshian, A., Z. Wang, G. Feingold, and T. S. L'Ecuyer (2013), A satellite perspective on cloud water to rain water conversion rates and relationships with environmental conditions, *J. Geophys. Res. Atmos.*, *118*, 6643–6650, doi:10.1002/jgrd.50523.

1. Introduction

[2] The nature and magnitude of aerosol-cloud-precipitation interactions remain poorly understood partly because of the dependence of such interactions on meteorological and thermodynamic regimes, cloud types, air mass characteristics, and data collection/analysis techniques and limitations [e.g., *Gultepe et al*., 1996; *Cahalan et al*., 2001; *Pawlowska and Brenguier*, 2003; *Comstock et al*., 2004; *Loeb and Manalo-Smith*, 2005; *Mauger and Norris*, 2007; *Loeb and Schuster*, 2008; *Kubar et al*., 2009; *Grandey and Stier*, 2010; *Su et al*., 2010; *Duong et al*., 2011]. One particular aspect of these interactions in warm clouds that is poorly understood is the collision-coalescence process between drops and the rate at which cloud water is converted to rain water (termed "conversion" hereinafter). Uncertainties in the conversion rates required to produce precipitation motivate a more detailed understanding of what controls this quantity, with the goal of improving its treatment in models.

[3] A number of environmental factors govern the time scale of warm rain production in clouds, including meteorology, thermodynamics, cloud dynamics, and aerosol properties. The microphysical underpinnings of aerosol-cloud-precipitation interactions in warm (liquid-only) clouds are widely accepted: an increase in aerosol concentration leads to a reduction in drop size (all else fixed) [*Twomey*, 1977], which suppresses precipitation production owing to less efficient collision-coalescence [*Warner*, 1968]. It is not clear whether these aerosol-related microphysical influences persist in extensive cloud fields, and over longer time scales, or whether they simply produce transient responses. For example, *Lee et al*. [2012] show how aerosol perturbations trigger changes in thermodynamic profiles that promote modifications in cloud vertical development that act to remove the differences. *Wood* [2007] also shows that changes in the sign of the aerosol indirect effects in marine stratocumulus clouds arise due to dissimilar response times for cloud base and cloud top heights. These results are congruent with the buffered aerosol-cloud system discussed in *Stevens and Feingold* [2009]. Ideas such as these motivate us to look to new data sets, specifically those from spaceborne remote sensors, to shed light on the extent of both aerosol and macrophysical influences on clouds.

[4] Satellite data can provide a global view of the conversion process and its sensitivity to environmental conditions. One way to examine the influence of environmental conditions on conversion is to apply a method introduced by *Stephens and Haynes* [2007], which leverages NASA A-Train satellite data [*Stephens et al*., 2002; *L'Ecuyer and Jiang*, 2010]. Their method of estimating conversion rates and associated time scales showed that the characteristic conversion time scale

Additional supporting information may be found in the online version of this article.

[1]Department of Chemical and Environmental Engineering, University of Arizona, Tucson, Arizona, USA.
[2]Department of Atmospheric Sciences, University of Arizona, Tucson, Arizona, USA.
[3]Earth Systems Research Laboratory, NOAA, Boulder, Colorado, USA.
[4]Department of Atmospheric and Oceanic Sciences, University of Wisconsin, Madison, Wisconsin, USA.

Corresponding author: A. Sorooshian, University of Arizona, PO BOX 210011, Tucson, AZ, 85721, USA. (armin@email.arizona.edu)

2169-897X/13/10.1002/jgrd.50523

Table 1. Summary of Aerosol Type Binning Criteria Using Threshold Values of Aerosol Optical Depth (AOD), Fine Mode Fraction (FMF), and Ångstrom Exponent (Å)[a]

Aerosol Category	AOD	Angstrom Exponent	FMF
Clean Fine	<0.1	>1	>0.7
Pollute Fine	>0.1	>1	>0.7
Clean Coarse	<0.1	<1	<0.3
Polluted Coarse	>0.1	<1	<0.3

[a]Although the term "polluted" is used, it does not always correspond to high particle number concentrations; for example, "polluted coarse" can represent air masses with very large particles that may have a similar particle number concentration as compared to the "clean fine" category.

for warm marine clouds varied predominantly between 5.6 min and 3 h between June and August of 2006, with 73% of their data set suggesting times longer than 26 min. The novel application of spaceborne data in that work provided a meaningful link to current regional and global scale models. The goal of this work is to extend the work of *Stephens and Haynes* [2007] by using A-Train satellite data to examine the warm cloud conversion process and its relationship with environmental conditions over the marine regions of the globe. The structure of this paper is as follows: (i) overview of data sets; (ii) summary of the method to quantify conversion rates and time scales; (iii) examination of global maps of quantities associated with conversion and relevant environmental parameters; (iv) quantification of relationships between aerosol properties, lower tropospheric static stability (LTSS), and conversion as a function of liquid water path (LWP); and (v) conclusions.

2. Data Sets

[5] Collocated aerosol, cloud, and precipitation data from the A-Train are used over a period of two full years (2007 – 2008). A detailed description of the satellite products employed is provided elsewhere [*Lebsock et al*., 2008; *Haynes et al*., 2009; *L'Ecuyer et al*., 2009]. Data from the CloudSat cloud profiling radar (1.4×1.8 km) are used to isolate single-layer warm-rain clouds over oceans and for values of mean cloud-layer reflectivity ($\overline{Z}$) and precipitation rate (R) [2C-PRECIP-COLUMN product; *Haynes et al*., 2009]. *Lebsock et al*. [2008] provide a detailed explanation of the screening methodology to select only warm clouds. This work examines precipitating scenes ($R \geq 0.01$ mm h^{-1}) with different $\overline{Z}$ thresholds between -15 and 0 dBZ.

[6] Near-simultaneous, collocated measurements of aerosol and cloud microphysical properties from MODIS are used with CloudSat data. Cloud properties include the drop effective radius (r_e; 3.7 μm channel) and cloud optical depth (τ_c), which are Level 2 MODIS products at 1 km resolution [*Platnick et al*., 2003]. The 3.7 μm channel is used for r_e as it has been shown to be more representative of cloud top radius as compared to the 2.1 or 1.6 μm channels [*Lebsock et al*., 2011]. Cloud LWP is estimated using the following relationship: $\mathrm{LWP} = 5/9 \times \rho_w \times \tau_c \times r_e$ [e.g., *Wood and Hartmann*, 2006].

[7] Remote sensing measurements have previously been used to identify aerosol types based on binning aerosol data sets by aerosol optical depth (AOD), fine mode fraction (FMF), and Ångstrom exponent (Å) [e.g., *Eck et al*., 1999; *Dubovik et al*., 2002; *Kaufman et al*., 2002; *Barnaba and Gobbi*, 2004]. AOD is a measure of columnar aerosol extinction, while the effect of aerosol size is captured by Å and FMF, the latter being defined as the ratio of fine mode AOD to total AOD. AI is thought to be a better proxy for CCN concentrations as compared to AOD [e.g., *Nakajima et al*., 2001]. Table 1 summarizes how these three aerosol parameters, based on $1^\circ \times 1^\circ$ gridded MODIS aerosol data (Level 3, MODIS Collection 5) [*Remer et al*., 2005], are used to define four aerosol types referred to as "clean fine," "clean coarse," "polluted fine," and "polluted coarse." It is cautioned that "polluted" does not always correspond to high particle number concentrations; for example, "polluted coarse" can represent air masses with very large particles that may have a lower total particle number concentration than the "clean fine" category. The use of aerosol data over a much larger spatial scale ($1^\circ \times 1^\circ$) as compared to cloud data (~ 1–2 km) is intended to reduce issues associated with aerosol swelling near cloud boundaries [e.g., *Haywood et al*., 1997; *Lebsock et al*., 2008; *Chand et al*., 2012].

[8] Data for low-level wind speeds are derived from the Advanced Microwave Scanning Radiometer (AMSR-E). LTSS data are derived from the European Center for Medium Range Weather Forecast-AUXiliary (ECMWF-AUX) products that are available at the CloudSat data processing center. The native ECMWF data resolution is 0.5°, and these data are linearly interpolated to the CloudSat footprint in space and time as described elsewhere [*Partain*, 2007]. LTSS represents a proxy for the thermodynamic state of the atmosphere [*Klein and Hartmann*, 1993; LTSS = potential temperature difference between 700 hPa and 1000 hPa].

3. Quantifying Conversion Rates and Time Scales

[9] The procedure developed by *Stephens and Haynes* [2007] to estimate conversion rates and characteristic time scales relies on the differing sensitivities of passive MODIS and active CloudSat radar observations. Conversion can be viewed as having contributions from both autoconversion (a drop concentration-dependent process) and accretion (which has negligible drop concentration dependence) with unknown relative weights. The critical assumption is that the droplet liquid water content and associated visible extinction properties derive from a smaller cloud droplet mode ("S1"; diameter ~2 to 47 μm), whereas the collecting drops, drizzle flux, and radar reflectivity derive from a larger mode ("S2"; diameter ~40 – 640 μm) [*Stephens and Haynes*, 2007; see their Figures 1 and 2]. The derivation of the vertically integrated conversion rate invokes the use of the Long collection kernel for droplet radii ≤50 μm, $K(R, r) \approx \kappa_2 R^6$ [*Long*, 1974], where κ_2 is 1.9×10^{11} cm^{-3} s^{-1}. This collection kernel is substituted in the following equation for the conversion rate, P:

$$P = \kappa_2 \int_{S2} N(R) R^6 \, dR \int_{S1} m(r) n(r) \, dr \qquad (1)$$

where $N(R)$ represents the size distribution of collector drops of radius R, $m(r)$ is the mass of smaller drops of radius r, $n(r)$ is the size distribution of smaller drops of radius r, and the two integration limits correspond to the two droplet modes. After additional simplification, equation (1) becomes:

$$P = \kappa_2 N R_6^6 L H [R_6 - R_{6c}] \qquad (2)$$

where L ($= \frac{4\pi}{3} \rho_w N_{S1} r_3^3$; r_3 = mean radius of third moment of S1) is the liquid water content associated with S1, H is the

Table 2. Average Values for Conversion Rate, LWP, AI, and LTSS for the Eight Subregions Shown in Figure 1a

	Conv. Rate ($g\,m^{-2}\,s^{-1}$)		LWP ($g\,m^{-2}$)		AI		LTSS (°C)	
	No Upper R Limit	0.1 mm h^{-1} > R	No Upper R Limit	0.1 mm h^{-1} > R	No Upper R Limit	0.1 mm h^{-1} > R	No Upper R Limit	0.1 mm h^{-1} > R
TP	0.12	0.09	121.8	104.8	0.07	0.07	15.0	14.9
F NEP	0.09	0.05	151.7	120.1	0.09	0.09	18.9	19.0
ECT	0.12	0.07	147.1	115.7	0.09	0.10	17.4	17.3
F SEP	0.10	0.06	151.6	124.8	0.08	0.08	19.8	19.9
GM	0.12	0.10	125.0	106.6	0.10	0.10	14.3	14.2
WA	0.10	0.05	155.3	126.8	0.25	0.20	18.5	18.3
IO	0.13	0.09	127.6	102.4	0.11	0.11	14.3	14.2
AC	0.12	0.09	138.8	109.8	0.15	0.13	15.0	15.0

Heaviside step function to account for a negligible conversion process when $R_6 < R_{6c}$, and R_6 is the mean radius of the sixth moment of S2. When considering that the larger S2 distribution is represented by CloudSat radar reflectivity $\left(Z = 64N_{S2}r_6^6\right)$, the vertically integrated conversion rate becomes:

$$P{\cdot}h = c_1\frac{5}{9}\rho_w r_e \tau_c \overline{Z} H[Z - Z_c] \tag{3}$$

where $P \cdot h$ $(= \int Pdh)$, h is cloud depth, $c_1 = \kappa_2/64$, L from equation (2) is substituted with $5/9 \times \rho_w \times \tau_c \times r_e$, $\overline{Z}$ is the cloud layer-mean radar reflectivity, and the Heaviside function is changed to reflect a negligible conversion process when $\overline{Z}$ is less than −15 dBZ (= Z_c). This threshold critical value of Z_c is derived from *Matrosov et al*. [2004] and *Wood* [2005]. We also employ another independent Heaviside function ($r_e > 12\,\mu m$) following work suggesting that there may be a threshold drop size required for the onset of precipitation [e.g., *Rosenfeld and Gutman*, 1994; *Han et al*., 1995; *Rosenfeld and Lensky*, 1998; *Ferek et al*., 2000; *Kobayashi*, 2007]. It will be shown that the conclusions herein remain robust, independent of which Heaviside function is used. The majority of the discussion will be based on the use of $H[Z - Z_c]$. The ratio of cloud LWP (units = $g\,m^{-2}$) versus the $P \cdot h$ term (units = $g\,m^{-2}\,s^{-1}$) provides an estimate of the characteristic time scale of the conversion process. Since conversion rate and the associated time scale represent different views of the same cloud process, this work focuses mainly on the conversion rate with only brief mention of time scales in section 4.2.

[10] The initial analysis of *Stephens and Haynes* [2007] used an upper $\overline{Z}$ limit of 0 dBZ and an upper R limit of 0.3 mm h^{-1} to (i) distinguish light and moderate drizzle, (ii) isolate clouds in their incipient stages of precipitation development, and (iii) attempt to view clouds with characteristic drizzle drop radii less than 50 μm. While it is difficult to unambiguously prove that clouds are in their incipient stages of rain development, a number of different upper $\overline{Z}$ and R limits are used to explore the sensitivity of results. We use multiple upper $\overline{Z}$ limits (0, −2.5, −5 dBZ). The associated upper R limit for each $\overline{Z}$ upper limit is informed by *Z-R* relationships based on stratocumulus measurements [*van Zanten et al*., 2005, Table 2]: $R = aZ^n$, where $a = 2.73 \pm 0.07$ and $n = 0.68 \pm 0.01$. The calculated R values are rounded down to obtain the following upper limits: $\overline{Z}$ = 0 dBZ, $R = 0.1$ mm h^{-1}; $\overline{Z}$ = −2.5 dBZ, $R = 0.07$ mm h^{-1}; $\overline{Z} = -5$ dBZ, $R = 0.05$ mm h^{-1}. These results are also compared with those using no upper R limit.

[11] This analysis is concerned with *relative* differences between different regions, LTSS conditions, and the presence of aerosol types. This reduces the influence of assumptions in the conversion calculations. Results that are sensitive to the presence of different aerosol types cannot unambiguously point to causal relationships, but rather can suggest that the presence of an aerosol type and other conditions covarying with its presence have an effect on conversion.

4. Results and Discussion

4.1. Spatial View of Conversion and Environmental Conditions

[12] Figures 1a and 1b show global maps of average conversion rate in individual 10° × 10° cells. These two figures consider data when $-15 < \overline{Z}$ (dBZ) < 0, with the difference being the upper R limit (Figure 1a: no upper R limit; Figure 1b: upper limit of 0.1 mm h^{-1}). The spatial patterns for conversion rate are the same, and the values in the two maps are highly correlated (r = 0.82, n = 357), indicating that the use of an upper R limit does not alter relative spatial differences. Conversion rates are systematically lower when using the upper R limit with a global maritime average (± standard deviation) of $0.07 \pm 0.02\,g\,m^{-2}\,s^{-1}$ and a range of $0.003 - 0.22\,g\,m^{-2}\,s^{-1}$. With no upper R limit, the average and range are $0.11 \pm 0.04\,g\,m^{-2}\,s^{-1}$ and $0.003 - 0.50\,g\,m^{-2}\,s^{-1}$, respectively. Although not shown in Figure 1, conversion rates were quantified for an upper R limit of 0.3 mm h^{-1} following *Stephens and Haynes* [2007]; similar spatial differences were observed as in Figure 1 with an average of $0.09 \pm 0.03\,g\,m^{-2}\,s^{-1}$ and range of $0.003 - 0.22\,g\,m^{-2}\,s^{-1}$. The conversion rates in this work lie within the range calculated by *Stephens and Haynes* [2007]. (Note that they used a different time span: June – August 2006.) The results suggest that lower R limits coincide with slower conversion rates due to clouds being earlier in their growth stages.

[13] Table 2 reports average conversion rates for specific regions defined in Figure 1a. Although results are reported both with and without use of an upper R limit, the discussion below is based on the latter condition. The three subtropical subsidence regions (Far Northeastern Pacific, Far Southeastern Pacific, and off the Western African coast) with the highest LTSS (18.5°C – 19.8°C) and LWP ($152 - 155\,g\,m^{-2}$) exhibit the lowest conversion rates ($0.09\,g\,m^{-2}\,s^{-1}$, $0.10\,g\,m^{-2}\,s^{-1}$, and $0.10\,g\,m^{-2}\,s^{-1}$, respectively). Conversely, the regions with the lowest LTSS (14.3°C – 15.0°C) and LWP ($122 - 139\,g\,m^{-2}$) (Tropical Pacific, Indian Ocean, Gulf of Mexico, Asian outflow) exhibit among the highest conversion rates ($0.12 - 0.13\,g\,m^{-2}\,s^{-1}$).

[14] Figure 2 reports global conversion rate maps for two LWP bins ($\leq 100\,g\,m^{-2}$ and $150 - 350\,g\,m^{-2}$) to identify if

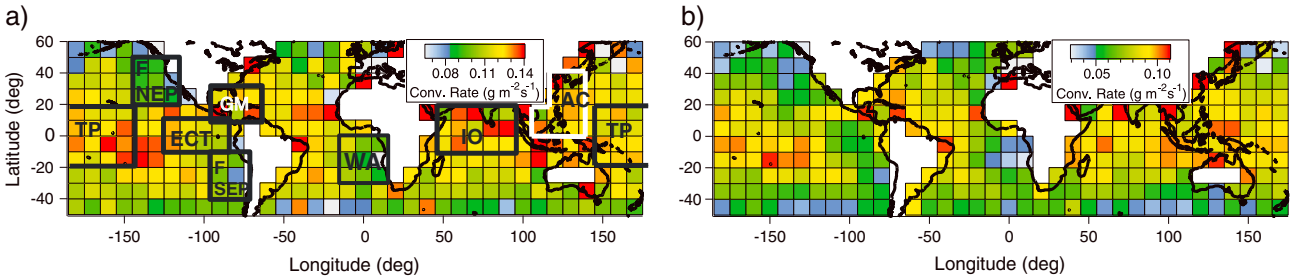

Figure 1. Spatial map of (a) conversion rate for data with the following conditions: $-15 < \overline{Z}\,(\mathrm{dBZ}) < 0$ and no upper R limit; Figure 1b same as Figure 1a except the upper R limit is 0.1 mm h^{-1}. The highlighted regions in Figure 1a are examined more closely in Table 2: TP = Tropical Pacific, F NEP = Far Northeastern Pacific, ECT = Equatorial Cold Tongue, F SEP = Far Southeastern Pacific, GM = Gulf of Mexico, WA = Western Africa, IO = Indian Ocean, AC = Asian Coast.

regional differences in Figure 1 are preserved when separating the data set into two bins of a parameter that has significant control over conversion. Conversion rates exhibit statistically significant correlations (two-tailed Student's t test at 95% confidence) spatially when comparing results from Figure 1a to high and low LWP bins in Figure 2 ($r \geq 0.62$; $n = 353$). Furthermore, conversion rates for both high and low LWP conditions exhibit statistically significant correlations with each other ($r = 0.60$; $n = 345$). Therefore, spatial trends are largely preserved for varying LWP binning conditions. Average global conversion rates for the low and high LWP conditions are $0.04 \pm 0.01\,\mathrm{g\,m^{-2}\,s^{-1}}$ and $0.20 \pm 0.06\,\mathrm{g\,m^{-2}\,s^{-1}}$, respectively. A reason why Table 2 shows higher conversion rates for regions with lower average LWPs is that there are competing effects of other covarying factors such as LTSS. The individual influence of LWP and LTSS is discussed in section 4.2.

[15] Estimates of autoconversion and accretion rates from aircraft measurements in drizzling stratiform clouds (assuming a 500 m thick cloud) tend to be smaller than those in Figure 1 [*Wood*, 2005]. Even when using reduced values for the upper $\overline{Z}$ limit and imposing upper R limits, average global conversion rates still are appreciable ($\overline{Z} < -2.5$ dBZ, $R < 0.07$ mm h^{-1}: $0.05 \pm 0.01\,\mathrm{g\,m^{-2}\,s^{-1}}$; $\overline{Z} < -5$ dBZ, $R < 0.05$ mm h^{-1}: $0.04 \pm 0.01\,\mathrm{g\,m^{-2}\,s^{-1}}$) and higher than those of the aforementioned study. A direct comparison would suggest that clouds in the satellite data set are likely beyond their earliest stages of rain production and are already raining appreciably. Accretion would be expected to be the dominant rain production mechanism, which would be consistent with the findings of *Wood* [2005] that autoconversion is significant only in the top 20% of stratiform clouds. However, some of the differences in absolute values may originate from the different estimation methods and data sets.

[16] Spatial maps of environmental factors that influence the conversion process are shown in Figure 3 using the same conditions as in Figure 1a ($-15 < \overline{Z}\,(\mathrm{dBZ}) < 0$, no upper R limit). Similar spatial trends and correlations exist when using an R limit of 0.1 mm h^{-1} (refer to Figure S1). The best predictors of conversion rate when performing a backward stepwise linear regression using $\overline{Z}$ and the parameters in Figure 3 include $\overline{Z}$ followed by LWP, LTSS, AI, AOD, and then FMF (model $r^2 = 0.82$, $n = 362$). Consequently, the parameters best correlated with conversion rate are LWP ($r = 0.43$), LTSS ($r = -0.35$), and $\overline{Z}$ ($r = 0.75$). Conditions of reduced atmospheric stability coincide with higher conversion rates, likely because of conditions more conducive to convection that allow for more active collision-coalescence. For example, the Indian Ocean subregion has the highest conversion rate ($0.13\,\mathrm{g\,m^{-2}\,s^{-1}}$) and lowest average LTSS (14.3°C) in Table 2.

[17] AOD levels are expectedly highest near the continental areas of Africa and Asia owing to the strong influence of dust, biomass burning, and anthropogenic pollution. AOD exhibits a weak correlation with conversion rate ($r = 0.06$). AI is negatively correlated with conversion rate ($r = -0.14$); the link between more and finer aerosol particles and slower conversion rates will be discussed further below. Higher wind speeds lead to at least two effects important for conversion: (i) stronger moisture fluxes [e.g., *Nuijens et al.*, 2009]; and (ii) coarse sea spray particles that can act as giant CCN and expedite the broadening of drop distributions

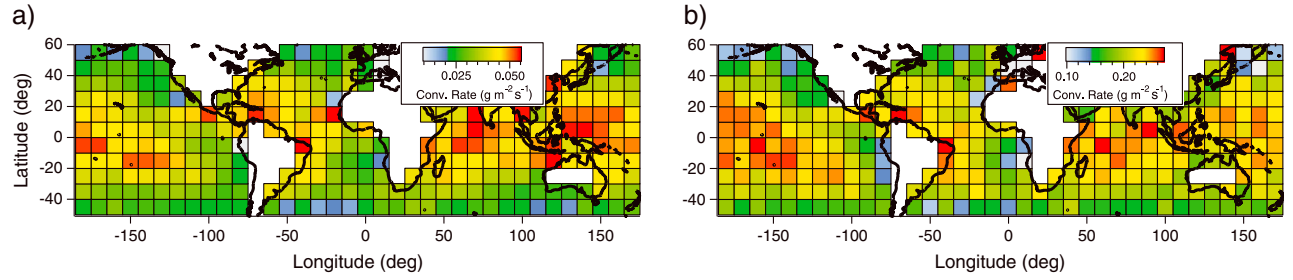

Figure 2. Spatial map of conversion rate for data in two LWP bins: (a) $\leq 100\,\mathrm{g\,m^{-2}}$ and (b) $\geq 150\,\mathrm{g\,m^{-2}}$. In addition, data in both panels meet the following conditions: $-15 < \overline{Z}\,(\mathrm{dBZ}) < 0$ and no upper R limit.

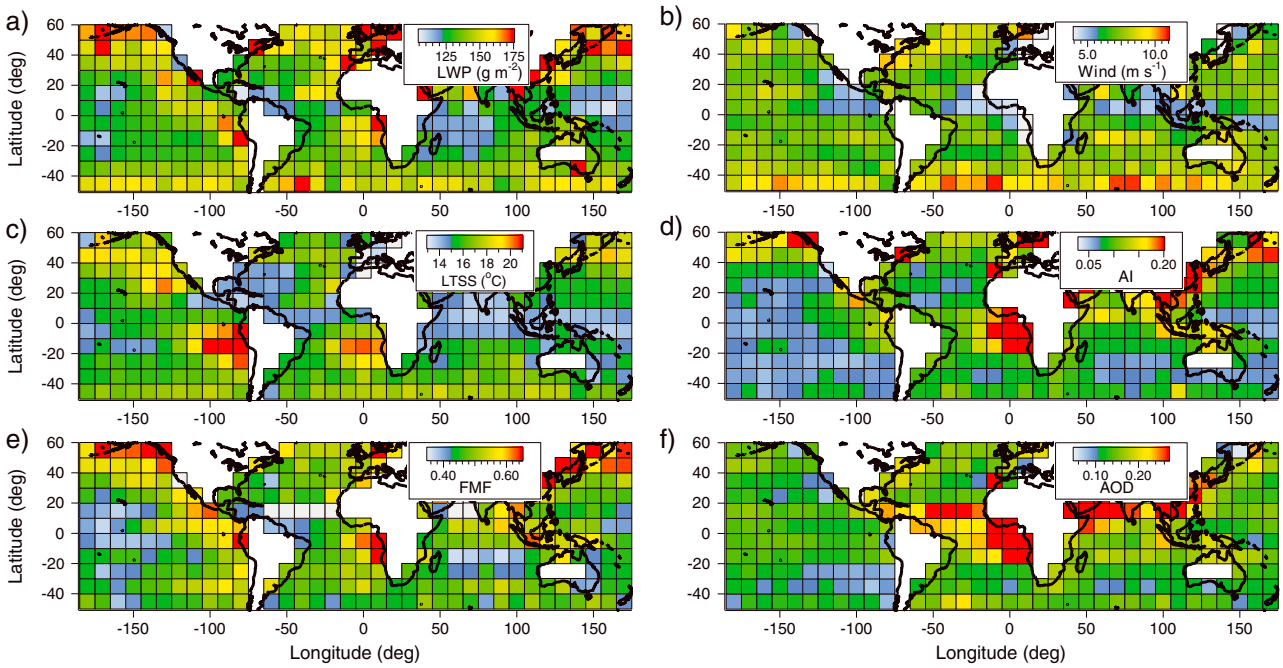

Figure 3. Spatial maps of average values of (a) LWP, (b) wind speed, (c) LTSS, (d) AI, (e) FMF, and (f) AOD. These data represent averages in $10^\circ \times 10^\circ$ pixels for warm precipitating clouds with LWP $< 350\ \mathrm{g\,m^{-2}}$, $-15 < \overline{Z}\ (\mathrm{dBZ}) < 0$, and no upper R limit.

[*Houghton*, 1938; *Johnson*, 1982]. However, wind speed shows a statistically significant negative relationship with conversion rate (r = −0.33). Wind speed and AOD show a similar spatial pattern, except in regions with strong influence from dust such as the Saharan Desert outflow region on the western side of Africa. Wind speed is best correlated, although negatively (r = −0.48), with FMF amongst the parameters in Figure 3. FMF exhibits higher values closer to continental regions owing to proximity to aerosol sources other than desert dust [e.g., *Kaufman et al.*, 2005]. The highest FMF levels coincide with regions in the northernmost part of Figure 1a that exhibit relatively low conversion rates.

[18] Prior to examining relationships between conversion rate and the presence of aerosol types in section 4.2, it is important to examine covarying factors with the presence of the four aerosol types. While specific statistics can be found in Table S1 for different upper R limit conditions, values are reported below for the global area in Figures 1–3 using no upper R limit. The aerosol types coinciding with the highest LTSS values are "clean fine" (17.0 ± 2.7°C) and "polluted fine" (17.7 ± 3.8°C), which are coincident with the lowest wind speeds ($4.2 \pm 1.7\ \mathrm{m\,s^{-1}}$ and $5.1 \pm 2.2\ \mathrm{m\,s^{-1}}$, respectively). "Clean coarse"/"polluted coarse" are coincident with LTSS and wind speeds of 15.7 ± 2.6°C/15.9 ± 2.5°C and $7.1 \pm 2.6\ \mathrm{m\,s^{-1}}$/$8.5 \pm 2.5\ \mathrm{m\,s^{-1}}$, respectively. The wind speed data are consistent with sea spray particles ("coarse") being more effectively ejected from the ocean surface at higher wind speeds. The highest average LWP is for the "polluted fine" category ($161\ \mathrm{g\,m^{-2}}$) while the other three have lower values ($143 - 147\ \mathrm{g\,m^{-2}}$). The highest r_e values are observed for the two "clean" categories (18.2 – 18.4 μm), with a maximum for the "clean coarse" type. The two "clean" categories coincide with the lowest AODs (0.05 – 0.07 versus 0.19 - 0.26 for the other categories), while "clean coarse" is characterized by the lowest AI value (0.02 ± 0.01, versus 0.03 – 0.33 for the other categories).

[19] It is hypothesized that the "clean coarse" category should coincide with the fastest conversion rates owing to a combination of the following: (i) fewer particles (and thus drops); (ii) the potential presence of large hygroscopic nuclei; and (iii) lower LTSS conditions and higher wind speeds (and presumably enhanced surface moisture fluxes) associated with this aerosol type can presumably promote more active conversion. Although the data set cannot show causal aerosol-cloud relationships, establishing whether the data are consistent with this hypothesis is of interest.

4.2. Relationship Between Conversion, Aerosol Types, and LTSS

[20] Figure 4 summarizes values of conversion rate as a function of LWP for each aerosol type in the northern hemisphere (0°N–60°N, 180°W–180°E). Three LWP bins between $0 - 350\ \mathrm{g\,m^{-2}}$ are used to strike a balance between holding a macrophysical parameter fixed and still having sufficient data points for the analysis in each bin. To separate the potential influence of aerosol type and LTSS, data are separated into two conditions of LTSS (<13.5°C and >21°C) to distinguish between stable and unstable conditions. These LTSS bins account for the lowest and highest 10 – 12% of the data set when using the following conditions: LWP $< 350\ \mathrm{g\,m^{-2}}$ and $-15 < \overline{Z}\ (\mathrm{dBZ}) < 0$. Four panels are shown in Figure 4 to present the sensitivity of conversion rate to the choice of the upper $\overline{Z}$ limit, the upper R limit, and the use of r_e or $\overline{Z}$ for the Heaviside function. (The reader is referred to Tables S2–S9 in the Supplementary Information for average/standard deviation/minimum/maximum values and sample size for each point

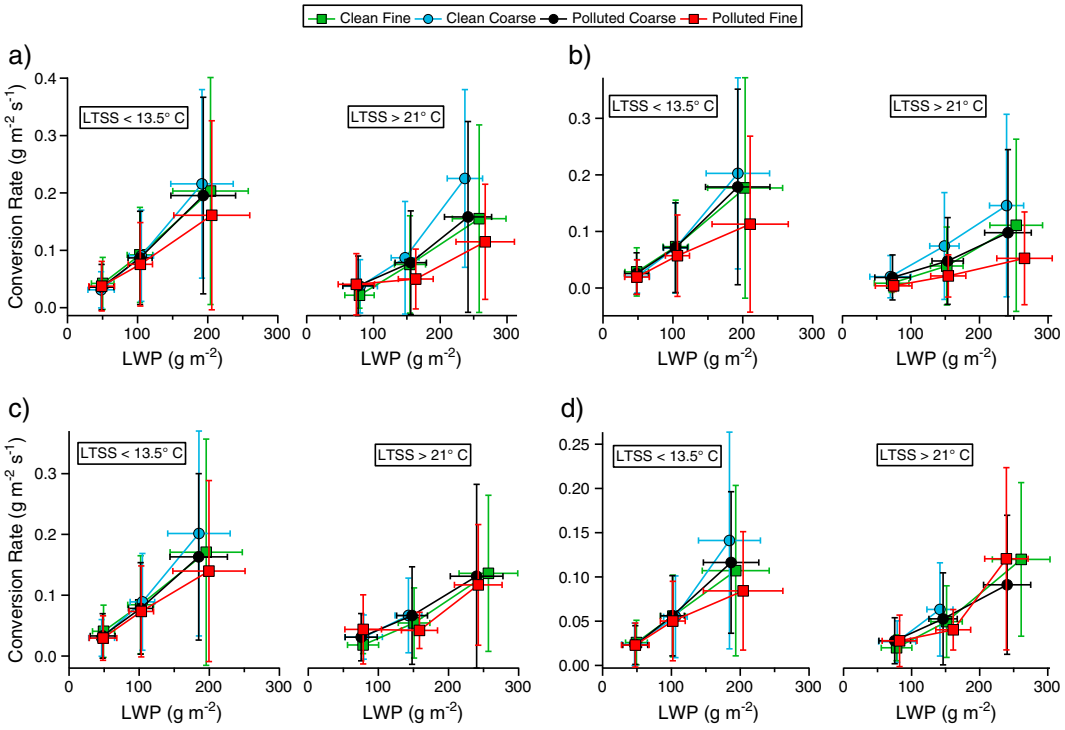

Figure 4. Conversion rate as a function of LWP for different combinations of aerosol types, and LTSS regimes for the northern hemisphere. The data used include the following conditions: (a) $-15 < \overline{Z}$ (dBZ) < 0 and no upper R limit; (b) $\overline{Z}$ (dBZ) < 0, and $r_e > 12\,\mu$m, no upper R limit; (c) $-15 < \overline{Z}$ (dBZ) < 0, upper R limit of 0.1 mm h^{-1}; and (d) $-15 < \overline{Z}$ (dBZ) < -2.5, upper R limit of 0.07 mm h^{-1}. Points are not included for "clean coarse" for high LTSS conditions in Figure 4c and 4d due to insufficient data points (<10).

shown in Figure 4 for the following parameters: conversion rate, LWP, AI, $\overline{Z}$, AOD, FMF, wind speed, r_e, LTSS.)

[21] Conversion rates expectedly increase as a function of LWP. This relationship is not evident in Table 2 most likely since LTSS was allowed to vary. Regardless of which Heaviside function is applied, the conversion rates are systematically higher for low LTSS conditions and trends with aerosol type are similar. The effect of reducing the upper $\overline{Z}$ limit is that conversion rate decreases. Imposing an upper R limit leads to reductions in conversion rates, similar to what is found when comparing Figures 1a and 1b.

[22] Clouds influenced by the aerosol types with lower AI values exhibit the highest conversion rate (at fixed LTSS) while the "polluted fine" type almost always exhibits the lowest conversion rate. This result supports the hypothesis that faster conversion is brought on by a combination of (i) fewer droplets (i.e. lowest AI values), (ii) potentially large hygroscopic nuclei that can expedite the broadening of the drop distribution (i.e., low FMF and Å), and (iii) lower LTSS conditions and higher wind speeds. These results are consistent with the findings of *L'Ecuyer et al.* [2009], who suggested that enhanced levels of sea salt particles over the ocean cause clouds to have an accelerated precipitation response, which they found to be more evident in low stability conditions. The slower conversion rate associated with the "polluted fine" category (at fixed LTSS) can be explained by the opposite of the three reasons above for the "clean coarse" category. The "polluted coarse" aerosol type has a faster conversion rate compared to "polluted fine" likely due to a large extent from having a lower number concentration of particles. Table S1 shows the large difference in AI values for these two categories (0.03 ± 0.02 versus 0.33 ± 0.26). These interpretations require additional research to improve the case for causality, which is a limitation with the current data set.

[23] Figure 5 reports conversion times as a function of LWP for the same conditions as in Figure 4a to provide the reader with a range of characteristic times. The times reported are the average (±standard deviation) of the

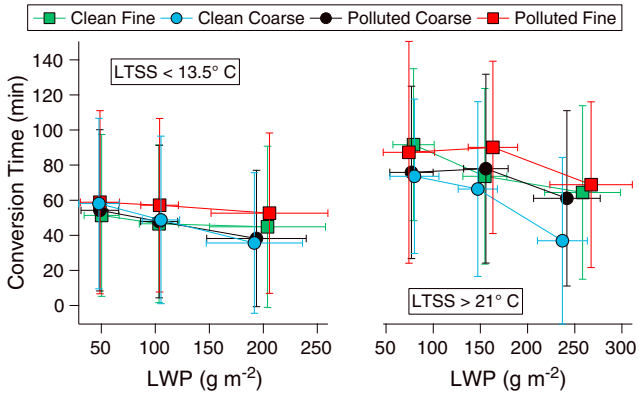

Figure 5. Conversion time as a function of LWP for different combinations of aerosol types and LTSS regimes for the northern hemisphere. The data used include the following conditions: $15 < \overline{Z}$ (dBZ) < 0 and no upper R limit.

LWP: $P \cdot h$ ratio for three different LWP bins. As expected, conversion times are fastest at low LTSS (36 – 59 min versus 37 – 92 min for high LTSS), they generally become faster at higher LWP, and are faster at lower AI conditions. The "clean coarse" category exhibits the fastest conversion times (36 – 58 min at low LTSS and 37 – 74 min at high LTSS), and "polluted fine" exhibits the longest times (53 – 59 min at low LTSS and 69 – 90 min at high LTSS).

5. Conclusions

[24] This study uses A-Train satellite data to examine the spatial distribution of warm cloud conversion rates and characteristic time scales. Emphasis is placed on examining relationships between LTSS, the presence of four different aerosol types, and AI with conversion. This analysis does not preclude the possibility that other environmental factors are also influential. The main findings of this work are as follows:

[25] 1. Warm cloud conversion rates are highest in regions with lower LTSS and in the presence of favorable aerosol types with low aerosol index values. The lowest conversion rates are shown to be in the southernmost and northernmost portions of the spatial area examined and near the subtropical subsidence regions off the western coasts of Africa, South America, and the United States.

[26] 2. The use of two criteria ($\overline{Z} > -15$ dBZ and $r_e > 12$ μm) to mark the onset of an active conversion process yields similar results for all analyses performed. The result of reducing the upper $\overline{Z}$ limit or imposing an upper R limit is to produce slower conversion rates presumably due to clouds being earlier in their growth stages. Regardless of the various calculation methods employed, the conversion rates exceed those of drizzling stratocumulus clouds derived from field data; therefore, the clouds studied in this work have a more active accretion process and/or the differences are likely a result of the different estimation methods and data sets.

[27] 3. "Clean coarse" conditions usually coincide with the highest coalescence rates and fastest conversion times potentially due to some combination of fewer droplets, the presence of large CCN, and favorable environmental conditions covarying with the presence of this aerosol type (e.g., low LTSS, stronger winds, and surface moisture fluxes). The "polluted fine" category exhibits the slowest conversion rates and longest conversion times most likely owing to higher LTSS, relatively low wind speeds, and more numerous and smaller drops in clouds that hamper the conversion process.

[28] Future work should examine the degree to which these conversion responses, if still robust with other and larger data sets, are driven by specific environmental conditions.

[29] **Acknowledgments.** This work was supported by NASA grant NNX12AC51G, NSF grant AGS-1008848, and an ONR YIP award (N00014-10-1-0811). GF acknowledges support from NOAA's Climate Goal. The authors acknowledge Matthew D. Lebsock, Daniel Rosenfeld, Robert Wood, and an anonymous reviewer for insightful comments related to this manuscript.

References

Barnaba, F., and G. P. Gobbi (2004), Aerosol seasonal variability over the Mediterranean region and relative impact of maritime, continental and Saharan dust particles over the basin from MODIS data in the year 2001, *Atmos. Chem. Phys.*, *4*, 2367–2391.

Cahalan, R. F., L. Oreopoulos, G. Wen, A. Marshak, S.-C. Tsay, and T. DeFelice (2001), Cloud characterization and clear sky correction from Landsat 7, *Remote Sens. Environ.*, *78*, 83–98.

Chand, D., R. Wood, S. J. Ghan, M. H. Wang, M. Ovchinnikov, P. J. Rasch, S. Miller, B. Schichtel, and T. Moore (2012), Aerosol optical depth increase in partly cloudy conditions, *J. Geophys. Res.*, *117*, D17207, doi:10.1029/2012JD017894.

Comstock, K., R. Wood, S. Yuter, and C. S. Bretherton (2004), Radar observations of precipitation in and below stratocumulus clouds, *Q. J. R. Meteorol. Soc.*, *130*, 2891–2918.

Dubovik, O., B. N. Holben, T. F. Eck, A. Smirnov, Y. J. Kaufman, M. D. King, D. Tanré, and I. Slutsker (2002), Variability of absorption and optical properties of key aerosol types observed in worldwide locations, *J. Atmos. Sci.*, *59*, 590–608.

Duong, H. T., A. Sorooshian, and G. Feingold (2011), Investigating potential biases in observed and modeled metrics of aerosol-cloud-precipitation interactions, *Atmos. Chem. Phys.*, *11*, 4027–4037.

Eck, T. F., B. N. Holben, J. S. Reid, O. Dubovik, A. Smirnov, N. T. O'Neill, I. Slutsker, and S. Kinne (1999), Wavelength dependence of the optical depth of biomass burning, urban, and desert dust aerosols, *J. Geophys. Res.*, *104*, 31,333–31,349, doi:10.1029/1999JD900923.

Ferek, R. J., et al. (2000), Drizzle suppression in ship tracks, *J. Atmos. Sci.*, *57*, 2707–2728.

Grandey, B. S., and P. Stier (2010), A critical look at spatial scale choices in satellite-based aerosol indirect effect studies, *Atmos. Chem. Phys.*, *10*(23), 11,459–11,470.

Gultepe, I., G. A. Isaac, W. R. Leaitch, and C. M. Banic (1996), Parameterizations of marine stratus microphysics based on in situ observations: Implications for GCMs, *J. Clim.*, *9*(2), 345–357.

Han, Q., W. Rossow, R. Welch, A. White, and J. Chou (1995), Validation of satellite retrievals of cloud microphysics and liquid water path using observations from FIRE, *J. Atmos. Sci.*, *52*, 4183–4195.

Haynes, J. M., T. S. L'Ecuyer, G. L. Stephens, S. D. Miller, C. Mitrescu, N. B. Wood, and S. Tanelli (2009), Rainfall retrieval over the ocean with spaceborne W-band radar, *J. Geophys. Res.*, *114*, D00A22, doi:10.1029/2008JD009973.

Haywood, J. M., V. Ramaswamy, and L. J. Donner (1997), A limited-area-model case study of the effects of sub-grid scale variations in relative humidity and cloud upon the direct radiative forcing of sulfate aerosol, *Geophys. Res. Lett.*, *24*(2), 143–146.

Houghton, H. G. (1938), Problems connected with the condensation and precipitation processes in the atmosphere, *Bull. Am. Meteorol. Soc.*, *19*, 152–159.

Johnson, D. B. (1982), The role of giant and ultragiant aerosol particles in warm rain initiation, *J. Atmos. Sci.*, *39*, 448–460.

Kaufman, Y. J., D. Tanré, and O. Boucher (2002), A satellite view of aerosols in the climate system, *Nature*, *419*, 215–223.

Kaufman, Y. J., I. Koren, L. A. Remer, D. Tanré, P. Ginoux, and S. Fan (2005), Dust transport and deposition observed from the Terra-Moderate Resolution Imaging Spectroradiometer (MODIS) spacecraft over the Atlantic Ocean, *J. Geophys. Res.*, *110*, D10S12, doi:10.1029/2003JD004436.

Klein, S. A., and D. L. Hartmann (1993), The seasonal cycle of low stratiform clouds, *J. Clim.*, *6*, 1587–1606.

Kobayashi, T. (2007), Significant differences in the cloud droplet effective radius between nonprecipitating and precipitating clouds, *Geophys. Res. Lett.*, *34*, L15811, doi:10.1029/2007GL29606.

Kubar, T. L., D. L. Hartmann, and R. Wood (2009), Understanding the importance of microphysics and macrophysics for warm rain in marine low clouds. Part I: Satellite observations, *J. Atmos. Sci.*, *66*(10), 2953–2972.

L'Ecuyer, T. S., W. Berg, J. Haynes, M. Lebsock, and T. Takemura (2009), Global observations of aerosol impacts on precipitation occurrence in warm maritime clouds, *J. Geophys. Res.*, *114*, D09211, doi:10.1029/2008JD011273.

Lebsock, M. D., G. L. Stephens, and C. Kummerow (2008), Multisensor satellite observations of aerosol effects on warm clouds, *J. Geophys. Res.*, *113*, D15205, doi:10.1029/2008JD009876.

Lebsock, M. D., T. S. L'Ecuyer, and G. L. Stephens (2011), Detecting the ratio of rain and cloud water in low-latitude shallow marine clouds, *J. Appl. Meteorol. Climatol.*, *50*(2), 419–432.

L'Ecuyer, T. S., and J. H. Jiang (2010), Touring the atmosphere aboard the A-Train, *Phys. Today*, *63*(7), 36–41.

Lee, S., G. Feingold, and P. Chuang (2012), Effect of aerosol on cloud environment interactions in trade cumulus, *J. Atmos. Sci.*, *69*, 3607–3632.

Loeb, N. G., and N. Manalo-Smith (2005), Top-of-atmosphere direct radiative effect of aerosols over global oceans from merged CERES and MODIS observations, *J. Clim.*, *18*, 3506–3526.

Loeb, N. G., and G. L. Schuster (2008), An observational study of the relationship between cloud, aerosol and meteorology in broken low-level cloud conditions, *J. Geophys. Res.*, *113*, D14214, doi:10.1029/2007JD009763.

Long, A. B. (1974), Solutions to droplet collection equation for polynomial kernels, *J. Atmos. Sci.*, *31*, 1040–1052.

Matrosov, S. Y., T. Uttal, and D. A. Hazen (2004), Evaluation of radar reflectivity-based estimates of water content in stratiform marine clouds, *J. Appl. Meteorol.*, *43*(3), 405–419.

Mauger, G. S., and J. R. Norris (2007), Meteorological bias in satellite estimates of aerosol-cloud relationships, *Geophys. Res. Lett.*, *34*, L16824, doi:10.1029/2007GL029952.

Nakajima, T., A. Higurashi, K. Kawamoto, and J. E. Penner (2001), A possible correlation between satellite-derived cloud and aerosol microphysical parameters, *Geophys. Res. Lett.*, *28*, 1171–1174, doi:10.1029/2000GL012186.

Nuijens, L., B. Stevens, and A. P. Siebesma (2009). The environment of precipitating shallow cumulus convection, *J. Atmos. Sci.*, *66*(7), 1962–1979.

Partain, P. (2007), Cloudsat ECMWF-AUX auxiliary data process description and interface control document, http://www.cloudsat.cira.colostate.edu/dataICDlist.php?go=list&path=/ECMWF-AUX.

Pawlowska, H., and J. L. Brenguier (2003), An observational study of drizzle formation in stratocumulus clouds for general circulation model (GCM) parameterizations, *J. Geophys. Res.*, *108*(D15), 8630, doi:10.1029/2002JD002679.

Platnick, S., M. D. King, S. A. Ackerman, W. P. Menzel, B. A. Baum, J. C. Riedi, and R. A. Frey (2003), The MODIS cloud products: Algorithms and examples from Terra, *IEEE Trans. Geosci. Remote Sens.*, *41*(2), 459–473.

Remer, L. A., et al. (2005), The MODIS aerosol algorithm, products, and validation, *J. Atmos. Sci.*, *19*(62), 947–973.

Rosenfeld, D., and G. Gutman (1994), Retrieving microphysical properties of cloud tops by multispectral analysis of AVHRR data, *J. Atmos. Res.*, *34*, 259–283.

Rosenfeld, D., and I. M. Lensky (1998), Satellite–based insights into precipitation formation processes in continental and maritime convective clouds, *Bull. Am. Meteorol. Soc.*, *79*, 2457–2476.

Stephens, G. L., and J. M. Haynes (2007), Near global observations of the warm rain coalescence process, *Geophys. Res. Lett.*, *34*, L20805, doi:10.1029/2007GL030259.

Stephens, G. L., et al. (2002), The Cloudsat mission and the A-Train, *Bull. Am. Meteorol. Soc.*, *83*, 1771–1790.

Stevens, B., and G. Feingold (2009), Untangling aerosol effects on clouds and precipitation in a buffered system, *Nature*, *461*, 607–613.

Su, W., N. G. Loeb, K. M. Xu, G. L. Schuster, and Z. A. Eitzen (2010), An estimate of aerosol indirect effect from satellite measurements with concurrent meteorological analysis, *J. Geophys. Res.*, *115*, D18219, doi:10.1029/2010JD013948.

Twomey, S. (1977), Influence of pollution on shortwave albedo of clouds, *J. Atmos. Sci.*, *34*, 1149–1152.

Warner, J. (1968), A reduction in rainfall associated with smoke from sugarcane fires—An inadvertent weather modification?, *J. Appl. Meteorol.*, *7*, 247–251.

Wood, R. (2005), Drizzle in stratiform boundary layer clouds. Part II: Microphysical aspects, *J. Atmos. Sci.*, *62*(9), 3034–3050.

Wood, R. (2007), Cancellation of aerosol indirect effects in marine stratocumulus through cloud thinning, *J. Atmos. Sci.*, *64*(7), 2657–2669.

Wood, R., and D. L. Hartmann (2006), Spatial variability of liquid water path in marine low cloud: The importance of mesoscale cellular convection, *J. Clim.*, *19*(9), 1748–1764.

van Zanten, M. C., B. Stevens, G. Vali, and D. H. Lenschow (2005), Observations of drizzle in nocturnal marine stratocumulus, *J. Atmos. Sci.*, *62*, 88–106, doi:10.1175/JAS-3355.1.